Modeling of the Outer Vestibule and Selectivity Filter of the L-Type Ca^{2+} Channel†

Gregory M. Lipkind‡ and Harry A. Fozzard*,§

Cardiac Electrophysiology Laboratories, Departments of Biochemistry and Molecular Biology and of Medicine, The University of Chicago, Chicago, Illinois 60637

Received February 7, 2001; Revised Manuscript Received April 3, 2001

ABSTRACT: Using the KcsA bacterial K^+ channel crystal structure [Doyle, D. A., et al. (1998) *Science 280*, 69−74] and the model of the outer vestibule of the Na^+ channel [Lipkind, G. M., and Fozzard, H. A. (2000) *Biochemistry 39*, 8161−8170] as structural templates, we propose a structural model of the outer vestibule and selectivity filter of the pore of the Ca^{2+} channel (α_{1C} or $Ca_v1.2$). The Ca^{2+} channel P loops were modeled by α-helix−turn−β-strand motifs, with the glutamate residues of the EEEE motif located in the turns. P loops were docked in the extracellular part of the inverted teepee structure formed by S5 and S6 α-helices with backbone coordinates from the M1 and M2 helices of the KcsA crystal structure. This construction results in a conical outer vestibule that tapers to the selectivity filter at the bottom. The modeled selectivity ring forms a wide open pore (∼6 Å) in the absence of Ca^{2+}. When Ca^{2+} is present (∼1 μM), all four glutamate side chains move to the center and form a cage around the dehydrated Ca^{2+} ion, blocking the pore. In the millimolar concentration range, Ca^{2+} also interacts with two low-affinity sites located externally and internally, which were modeled by the same carboxylate groups of the selectivity filter. Calculation of the resulting electrostatic potentials show that the single Ca^{2+} ion is located in an electrostatic trap. Only when three Ca^{2+} ions are bound simultaneously in the high- and low-affinity sites of the selectivity filter is Ca^{2+} able to overcome electrostatic attraction, permitting Ca^{2+} flux.

Voltage-gated Ca^{2+} channels belong to a structurally homologous superfamily of voltage-gated channels that includes the K^+ and Na^+ channels (*3*). Each channel type is distinguished by specific selective permeability for physiologically relevant cations. The L-type Ca^{2+} channel is permeable to divalent cations Ca^{2+}, Sr^{2+}, and Ba^{2+}, while rejecting monovalent ions by ratios of ∼1000:1 under physiological conditions (*3*). All of the voltage-gated channels share a common motif of four homologous domains or subunits (I−IV), each composed of six hydrophobic putative transmembrane segments (S1−S6) (*4*−*6*). Biophysical and biochemical data indicate that the extracellular segment between S5 and S6, usually called the P loop, folds back into the membrane to form the extracellular mouth of the pore and the selectivity region (*7*), while S6 and possibly S5 segments form most of the pore lining from the P loop to the intracellular side of the pore (*5*, *8*).

Recently, MacKinnon and colleagues have determined at 3.2 Å resolution the pore structure of a bacterial K^+ channel called KcsA (*1*). This K^+ channel has the characteristic selectivity of voltage-gated K^+ channels, but is not voltage-dependent. The protein subunits contain only two membrane-spanning segments, M1 and M2. Four subunits form the conducting pathway, lined by a "teepee" of converging M2 transmembrane helices. In accordance with prediction, the P loops between M1 and M2 are arranged to form the selectivity filter of the channel, which is 12 Å long and 3 Å in diameter. In the P loop, the main chain carbonyls of four or five highly conserved amino residues (TVGYG, the "signature sequence" for K^+ selectivity) face the pore, while their side chains face outward into the protein.

The outer vestibule and selectivity region of the Na^+ and Ca^{2+} channels must be different from the K^+ channel structure to account for their different selectivity properties. For the Na^+ channel, the side chains of a restricted number of amino acid residues form the selectivity filter (*5*, *9*−*13*), rather than the main chain carbonyls. Specifically, four highly conserved amino acids in the same relative position in the Na^+ channel P loops of domains I−IV participate in the formation of the selectivity filter, Asp-384, Glu-942, Lys-1422, and Ala-1714 (the DEKA motif), using the rat brain channel numbers. The P loops of domains I−IV of L-type Ca^{2+} channels contain a highly conserved pattern in positions corresponding to those of the DEKA motif (*14*, *15*). These residues are Glu-393, Glu-736, Glu-1145, and Glu-1446 (the EEEE motif), using the numbers of the rabbit cardiac L-type channel (rabbit $Ca_v1.2$). Surprisingly, it has been possible to switch the selectivity filter properties of the Na^+ and Ca^{2+} channels by mutation of the DEKA and EEEE motifs. Substitution of Lys-1422 and Ala-1714 in the Na^+ channel with Glu (DEEE) creates a mutant channel with a dramatic change in selectivity from Na^+ to Ca^{2+} (*14*). Moreover, the double mutant exhibited some characteristic pore behavior of native Ca^{2+} channels, including permeation by Na^+ in the absence of Ca^{2+}, but block of Na^+ permeation by

† Supported by Grant RO1 HL-65661.

* To whom correspondence should be addressed: MC 6094, University of Chicago Hospitals, 5841 S. Maryland Ave., Chicago, IL 60637. Telephone: (773) 702-1481. Fax: (773) 702-6789. E-mail: foz@hearts.bsd.uchicago.edu.

‡ Department of Biochemistry and Molecular Biology.

§ Department of Medicine.

10.1021/bi010269a CCC: $20.00
Published on Web 05/16/2001

micromolar levels of Ca^{2+} (*16*, *17*). Further, a double mutant of the Ca^{2+} channel, E1086K/E1387A (human L-type $Ca_v1.2$), in which two glutamic acids of the selectivity ring were substituted to mimic the Na^+ channel at equivalent positions exhibited pore properties similar to those of Na^+ channels by permeating Na^+ 15-fold more effectively than Ba^{2+} (*18*). These fundamental observations allow the conclusion that the EEEE locus is essential for ion selectivity in Ca^{2+} channels and that the basic pore structures of Na^+ and Ca^{2+} channels may be similar.

Substitution of single amino acids systematically in the EEEE motif of Ca^{2+} channels contribute to the high-affinity site for Ca^{2+}, with the carboxylate in the P loop of domain III having the strongest effect (*18*−*23*). Neutralization of any of the glutamates to a glutamine shifted the block of Li^+ current to much higher Ca^{2+} concentrations. Therefore, all four glutamate side chains form a binding site for Ca^{2+}. The accessibility of sulfhydryl-reactive agents with cysteine substitutions of the residues in the EEEE locus (*24*) also confirms that the side chains of these glutamates are likely to project into the pore, where they can interact with permeating ions. The interconversion of some selectivity functions between Na^+ and Ca^{2+} channels presumably reflects an underlying structural similarity of these channels, especially in the selectivity region, offering the chance for molecular modeling of Ca^{2+} channels. Modeling of the Na^+ channel outer vestibule has been more advanced, because of the availability of selective and very high affinity block by the structurally defined natural toxins, tetrodotoxin (TTX)[1] and saxitoxin (STX) (*3*, *25*).

We have recently described a molecular model of the pore of the Na^+ channel, combining an outer vestibule structure with a pore analogous to the crystal structure of the KcsA channel (*2*). The outer vestibule model (*12*, *26*) was based on site-directed mutagenesis data of parts of the P loops of domains I−IV (*9*, *27*) and the structures of the guanidinium toxins (*28*). The vestibule−pore model utilized the α-helix−turn−β-strand motif of P loops and the teepee structure of M1 and M2 of the KcsA channel for the analogous S5 and S6 helical segments (*1*), because the K^+ and Na^+ channels probably have a common genetic ancestry (*29*). Consequently, it is likely that the voltage-gated channels have a similar arrangement of their transmembrane segments, with specific adaptation of the selectivity filter region. Using this Na^+ channel pore as a template, we present a model of the Ca^{2+} channel pore, placing the EEEE motif in the same position as the DEKA motif of the Na^+ channel. This model predicts significant features of the Ca^{2+} channel selectivity and sieving properties and provides testable features of the pore. It also provides a candidate structural framework for molecular dynamics calculations on channel selectivity.

METHODS

Modeling was accomplished in the Insight and Discover graphical environment (MSI, Inc., San Diego, CA), as previously described (*26*). Molecular mechanics energetic calculations utilized the consistent valence force field approximation (cvff). For minimization procedures, the steepest descents and conjugate gradients were used. Calculations of electrostatic potentials inside the outer vestibule of Ca^{2+} channels was accomplished by the DelPhi module, based on the methodology described by Gilson and Honig (*30*). The dielectric constants were set to 10 for the protein interior and 80 for the solvent water region.

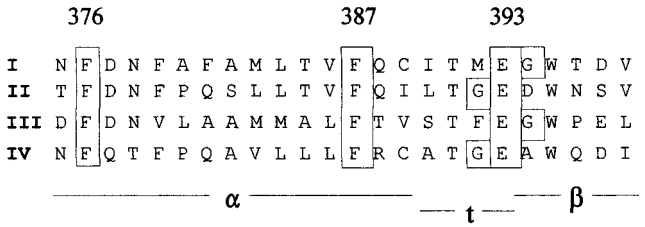

FIGURE 1: Alignment of the amino acid sequences of the P loops of domains I−IV of the Ca^{2+} channel ($Ca_v1.2$). The numbering corresponds to the P loop of domain I. Residues of the selectivity filter EEEE motif and the neighboring glycine residues are enclosed in boxes. The other highly conserved residue locations are also highlighted. At the bottom, the bar labeled α represents the proposed α-helical region, β represents the β-strand region, and t represents the inner turn of the P loops.

RESULTS AND DISCUSSION

In our presentation of the outer vestibule of the Na^+ channel (Figure 7 of ref *2*), P loops of domains I−IV were docked into the extracellular part of the inverted teepee structure formed by the C-terminal segments of S5 and the N-terminal segments of S6 helices that were spacially located by the coordinates of the KcsA M1 and M2 main chains (*1*). As a result, each P loop formed densely packed contacts with α-helices of S5 and S6 segments of its own domain and S6 of the neighboring domain. The domains were arranged clockwise, as supported by our studies of the interactions of the guanidinium toxins (*12*) and μ-conotoxin (*31*). No direct information about domain orientation is available for the Ca^{2+} channel, so we followed the clockwise arrangement of the Na^+ channel. The first steps in reconstructing the pore of the Ca^{2+} channel require alignment of the amino acids of P, the S5 and S6 sequences corresponding to those of the KcsA channel and the Na^+ channel, respectively.

P Loops. Alignment of the P loop amino acids of the Na^+ channel (*4*) and L-type Ca^{2+} channels (*15*) by the putative selectivity filter residues shows that they contain a region of highly conserved hydrophobic residues just N-terminal to the selectivity filter (Figure 1 and also Figure 1 of ref *2*). For domain I of the Na^+ channels, these correspond to residues 386−394 ($Na_v1.4$ numbering), and for domain I of the Ca^{2+} channels, they are residues 379−387 ($Ca_v1.2$ numbering). Noteworthy are the very conserved Phe or Tyr residues in two positions in both channel types (positions 376 and 387 in $Ca_v1.2$) and the Trp (position 395) that reflect unique amino acid sequence homology between domains and channel types, suggesting that the two P loop types have the same structural motifs. The hydrophobic character of these sequences N-terminal to the selectivity filter and the high proportion of α-helix-forming residues (Ala, Leu, Phe, and Met; *32*) encourages their modeling as α-helices (*33*, *34*). Typically, the N-terminal ends of α-helices show a

[1] Abbreviations: TTX, tetrodotoxin; STX, saxitoxin; $Ca_v1.2$, α1-subunit of the cardiac Ca^{2+} channel; $Na_v1.4$, α-subunit of the skeletal muscle Na^+ channel isoform; MTSET, methanethiosulfonate ethyltrimethylammonium; TMA, tetramethylammonium.

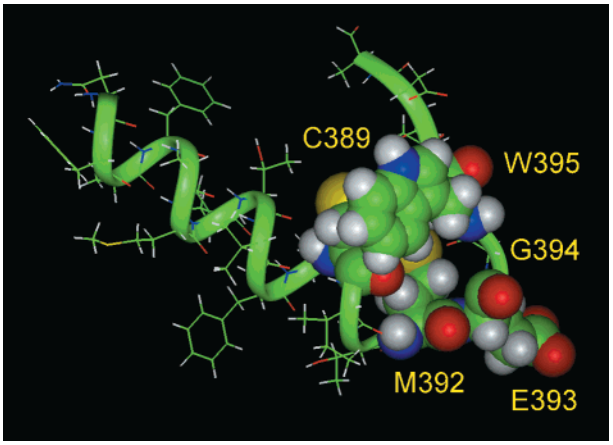

FIGURE 2: α-Helix−turn−β-strand conformation of the Ca^{2+} channel domain I P loop. The inner hydrophobic core that stabilizes the structure is formed by the side chains of residues Cys-389, Met-392, and Trp-395, which are shown as space-filling images. Glu-393, which participates in the formation of the selectivity filter, is also distinguished.

preference for Ala, Glu, and Asn and the C-terminal ends for Arg, Lys, and Gln (*32*), suggesting that the P helix includes residues 375−389. The P loops were therefore modeled, as for Na^+ channels, as α-helix−turn−β-strand motifs with residues of the selectivity filter at the beginning of the β-strands. This motif is a common type of structural organization, with a hydrophobic residue on one side of the β-strand fitting into a hydrophobic pocket in the α-helix (*35*, *36*) to stabilize the αβ-structure of the P loops. As suggested for the KcsA channel (*1*), the P loop α-helix would produce a dipole field, focused at the turns and the selectivity filter.

The optimized structure of the Ca^{2+} channel domain I P loop is shown in Figure 2. Here the inner hydrophobic core is formed by the side chains of amino acid residues Cys-389, Met-392, and Trp-395. The other P loops were organized in the same manner. Residues of the EEEE locus face the pore after the turns and form the first residues of the C-terminal β-strands. All Ca^{2+} channels contain conserved glycine residues in neighboring positions. In domains II and IV, these glycines precede Glu residues, while in domains I and III, they follow Glu residues so that they occupy positions −1 or 1 relative to the selectivity filter (Figure 1). Taking into account the high conformational preference of Gly residues to be included in reverse turns of peptide chains (*32*, *37*), we might expect the very conserved dipeptides GlyGlu and GluGly to participate in the formation of β-turns of the P loop hairpins and, consequently, to result in different conformations. Instead, the proposed construction maintains the symmetry of the Glu residues and locates the conserved Gly residues of repeats I and III inside the C-terminal β-strands, in positions preceding conserved Trp residues. There is also a tendency for Gly residues in αβ-fragments to be located not only in turns but also in positions preceding bulky hydrophobic residues (for example, Gly-228 before Trp-229 in triose phosphate isomerase; *38*). Most likely, the Gly residues in the proximity of the EEEE locus do not play specific conformational roles because all of these positions could be substituted with cysteine while maintaining channel function (*24*). When replaced with Cys, positions −1 were almost insensitive to the sulfhydryl-modifying agent MTSET, while the level of current reduction after interaction with MTSET was 60−80% for all position 1 residues (Gly-394, Asp-737, Gly-1146, and Ala-1447) substituted with Cys. Therefore, it is likely that the position 1 residues face the pore and adopt uniform locations in the selectivity region, while position −1 residues are removed from the center of the pore. Consequently, the glutamate residues of the EEEE locus can be arranged symmetrically on the same level of the pore, forming a single binding site for Ca^{2+} ions. An alternative alignment has been proposed by Varady et al. (*33*), placing glutamates of domains II and IV external to those of domains I and III, forming two distinct Ca^{2+} sites. This, however, contradicts the mutational data on Ca^{2+} channels (*22*) that showed that all of the glutamates participate in the high-affinity site.

S5 and S6 Alignment. The P loops of the Na^+ channel of the four domains are necessarily widely separated because of the dimensions of the pore-occluding guanidinium toxins (Figure 3 of ref *2*). A consequence of this separation is that the P loops do not have mutual van der Waals contacts, in contrast to the closely packed P loops of the KcsA channel (*1*). If it is assumed that the Ca^{2+} channel has a pore structure more like the Na^+ channel, the Ca^{2+} channel P loops require stabilization by nonbonded contacts with some other parts of the protein. One possibility for occupancy of the space between the P loops is the upper parts of the S6 segments.

As a first approximation, the S5 and S6 helices are arranged like the M1 and M2 helices of the KcsA channel, forming an external inverted teepee. For alignment of the S6 amino acids of the Ca^{2+} channel ($Ca_v1.2$) with those of the KcsA M2 and also with the $Na_v1.4$ isoform of the Na^+ channel, we can use drug interactions with the inner pore. Hockerman et al. (*39*, *40*) have shown for the L-type Ca^{2+} channel that mutations Y1463A, A1467S, and I1470A in domain IV S6 were less sensitive to block by the phenylalkylamine (−)D888, suggesting that these amino acids face the channel pore. Using this orientation, domain IV S6 could be aligned, locating Tyr-1463 and Ala-1467 in the pore-facing positions corresponding to Met-96 and Ile-100 of KcsA, and with Ile-1575 and Phe-1579 of $Na_v1.4$ (*2*) (Figure 3 and Figure 4 of ref *2*). The Phe-1454 at the beginning of the domain IV S6 α-helix (A. Stea et al., 1995) coincides with the N-end Trp-87 residue of the M2 α-helix (*1*).

Similar logic allows alignment of the S6 segment of domain III on the basis of coincidence of its Tyr-1152 with Tyr-1463 of domain IV (Figure 3); mutations of Tyr-1152 changed the affinity of $Ca_v1.2$ for binding of phenylalkylamines (*40*). For the S6 segments of domains I and II, mutagenesis information is absent, and their arrangement inside the pore was predicted on the basis of a high degree of homology with the alignment of S6 domains I and II of the Na^+ channel. As in the case of KcsA, the N-ends of S6 domains I and II helices of $Ca_v1.2$ are also bulky hydrophobic residues (Leu, Leu, Val, and Phe).

Less experimental evidence is available to assist in the alignment of S5 segments. We chose to assume that they contain conserved Gly residues inside the C-terminus ends (Figure 4), which we predict to play a structural role in docking the C-ends of the S5 helices with the bulky hydrophobic residues on the N-ends of the S6 helices to form the teepee structure. This permitted the formation of the inverted teepee motif for S5 and S6 of both Na^+ and Ca^{2+} channels using the crystal coordinates of M1 and M2, despite

KcsA	I	II	III	IV
Trp-87	Leu-410	Leu-758	Val-1143	Phe-1454
Gly	Pro	Val	Glu	Ala
Arg	Trp	Cys	Ile	Val
Leu	Val	Ile	Ser	Phe
Val	Tyr	Tyr	Ile	Tyr
Ala	Phe	Phe	Phe	Phe
Val	Val	Ile	Phe	Ile
Val	Ser	Ile	Ile	Ser
Val	Leu	Leu	Ile	Phe
Met-96	Val	Phe	Tyr-1152	Tyr-1463
Val	Ile	Ile	Ile	Met
Ala	Phe	Cys	Ile	Leu
Gly	Gly	Gly	Ile	Cys
Ile-100	Ser	Asn	Ile	Ala-1467
Thr	Phe	Tyr	Ala	Phe
Ser	Phe	Ile	Phe	Leu
Phe-103	Val	Leu	Phe	Ile-1470
Gly	Leu	Leu	Met	Ile
Leu	Asn	Asn	Met	Asn
Val	Leu	Val	Asn	Leu
Thr-107	Val	Phe	Ile	Phe
Ala	Leu	Leu	Phe	Val
Ala	Gly	Ala	Val	Ala
Leu	Val	Ile	Gly	Val
Ala	Leu	Ala	Phe	Ile
Thr	Ser	Val	Val	Met

FIGURE 3: Proposed alignment of S6 segments of domains I−IV of the Ca^{2+} channel with M2 of the KcsA channel. Some residues with the side chains facing the pore are enclosed in boxes. The pore-facing residues in domains III and IV were predicted on the basis of local anesthetic drug interactions within the pore.

I	I	A	L	L	V	L	F	V	I	I	I	Y	A	I	I	G	L	E	L	F
II	L	L	L	L	L	F	L	F	I	I	I	F	S	L	L	G	M	Q	L	F
III	I	V	I	V	T	T	L	L	Q	F	M	F	A	C	A	G	V	Q	L	F
IV	V	A	L	L	I	V	M	L	F	F	I	Y	A	V	I	G	M	Q	V	F

FIGURE 4: Alignment of amino acid sequences of S5 segments of domains I−IV of the Ca^{2+} channel. The conserved Gly residues, which are enclosed with boxes, establish the interaction between the C-ends of S5 and the N-ends of S6 α-helices.

differences in the residues and the lower confidence in the alignment of S5.

Ca^{2+} Channel Outer Vestibule. In the Na^+ channel model (*2*), the P loop N-end α-helices are in contact with S5 helices. That was the only way to locate the Na^+ channel P loops farther from the center of the pore, in the space between the S5 and S6 segments. This docking determined the location of the selectivity filter approximately at the level of Ile-1575 of domain IV S6, and resulted in a closed model of the outer vestibule and selectivity filter of the $Na_v1.4$ channel (Figure 7 of ref *2*), where the Lys-1237 side chain forms a hydrogen bond or salt bridge with Glu-755 of domain II and also interacts with Asp-400 of the opposite domain I through a water bridge. The Ca^{2+} channel vestibule also formed a densely packed structure at a similar location in the teepee transmembrane helical structure. Packing of each Ca^{2+} channel P loop into the spaces between the S5 and S6 helices of the same domain and S6 of the neighboring domain was accomplished by adjustment of the location and conformation of the residue side chains to avoid the more obvious van der Waals conflicts. The minimization of the potential energy of nonbonded interactions was made, determining the optimal

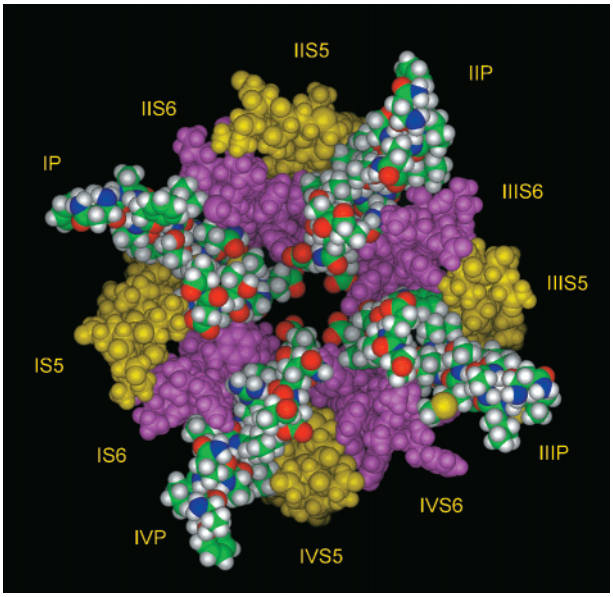

FIGURE 5: Model of the outer vestibule of the Ca^{2+} channel shown as space-filling images. The model includes α−β units of P loops with regular colors of the atoms and α-helices of S5 (yellow balls) and S6 (pink balls) segments of domains I−IV in a clockwise arrangement. Note that the P loops intercalate between the S6 segments of the four domains with the P loop α-helix also in contact with S5 of its own domain. A wide opening on the bottom represents the selectivity filter, formed by the side chains of glutamate residues of the EEEE motif.

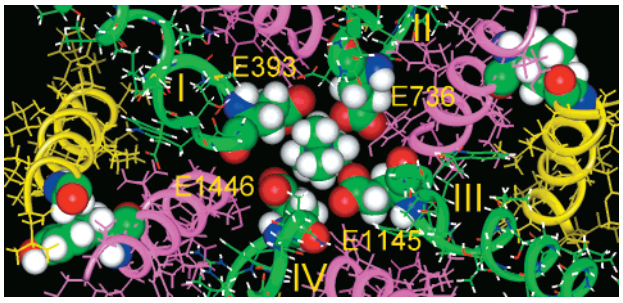

FIGURE 6: Model of the outer vestibule of the Ca^{2+} channel where the backbones of P loops and S5 and S6 α-helices are shown as green, yellow, and pink ribbons, respectively. Four amino acid residues of the selectivity filter, Glu-393, Glu-736, Glu-1145, and Glu-1446, produce an opening (~6 Å diameter) in the absence of external Ca^{2+}, which allows permeation of tetramethylammonium (TMA, shown in the center). The figure also shows close contacts between glycine residues on the C-ends of S5 α-helices with bulky hydrophobic residues on the N-ends of S6 α-helices.

arrangement for the four-domain assembly. Reconstruction of the $Ca_v1.2$ outer vestibule viewed from the outside is shown in Figures 5 and 6 by space-filling and ribbon images, respectively. As in the Na^+ channel model, the surface of the outer vestibule was formed by β-strands of the four P loops, which are held in position by their interactions with the P loop α-helices, and which in turn are held in position by their interaction with the S5 and S6 segments. This differs from the packing arrangement of the KcsA channel. Figure 6 also presents interactions of the conserved Gly residues of the S5 helices (Figure 4) with the bulky hydrophobic side chains of the neighboring S6 helices. For example, the Gly residue of S5 of domain III is in immediate contact with the side chain of Ile-1147 of the S6 α-helix. The backbones of the P loop α-helix−turn−β-strand motif were populated by $Ca_v1.2$ residues Glu-393, -736, -1145, and -1446 in the

positions analogous to the DEKA ring selectivity filter of the Na^+ channel. These residues are shown on the bottom by space-filled images (Figure 6).

This construction results in a conical outer vestibule with dimensions similar to those of the Na^+ channel, but without its outer ring of charged residues (Glu-403, Glu-758, Asp-1241, and Asp-1532). Instead, only hydrophobic or weakly polar amino acid residues (Thr-356, Asn-739, Pro-1148, and Gln-1449) face the pore at a corresponding level. Because for the Na^+ channel that charged ring is very important in interactions of TTX, STX, and μ-conotoxin (*9*, *12*, *41*, *42*), the proposed structure of the Ca^{2+} channel vestibule would not bind those toxins.

In the Na^+ channel outer vestibule model, the S6 segments do have immediate contact with selectivity filter residues. The domain IV S6 residue one helical turn above Phe-1579 is Ile-1575 (*43*), which is located by energy minimization at the level of the selectivity filter. It is notable that the Ca^{2+} channel residue analogous to the Na^+ channel Ile-1575 is Tyr-1463. Its mutation to Ala alters the reversal potential of the channel by −15 mV and increases the level of permeation of *N*-methyl-D-glucamine (*39*), suggesting that Tyr-1463 is indeed located in the proximity of the selectivity filter. The proposed alignment of S6 segments of domains I−IV of $Ca_v1.2$ (Figure 3) locates Tyr-1152 of domain III on the same level as Tyr-1463 inside the pore. Mutation of Tyr-1152 to Ala also altered selectivity (*40*). In the model of the Ca^{2+} channel outer vestibule (Figure 6), Tyr-1152 is located between the side chains of glutamic acids of the domain II and III selectivity filter (Glu-736 and Glu-1145), while Tyr-1463 is between Glu-1145 and Glu-1446 of domains III and IV. Tyr-1152 and Tyr-1463 also modulate the affinity for phenylalkylamines and dihydropyridines (*39*, *40*, *44*). The proximity of these residues to the selectivity filter suggests that they might interact with this critical region. Most likely, the protonated form of the phenylalkylamines can interact with the glutamatic acids of the selectivity filter (*40*). Dihydropyridines, containing strongly polarized NO_2 and C═O groups, could interact with Ca^{2+} inside the pore (*45*, *46*). The dihydropyridines and benzothiazepines approach their binding sites from the outside, while the phenylalkylamines access their site from the inside, supporting the idea that their overlapping sites must be near the selectivity filter.

Both Na^+ and Ca^{2+} channels are characterized by prominent sieving behavior. In the absence of external inorganic ions, the channels allow permeation of small organic cations and polar nonelectrolytes (*3*). Guanidine and aminoguanidine permeate the Na^+ channel, but not methylammonium. In contrast, not only methylammonium but also di-, tri-, and tetramethylammonium (TMA) permeate the Ca^{2+} channel (*47*, *48*). This has led to the conclusion that the Ca^{2+} channel selectivity filter has an opening equivalent to a 5.5 Å × 5.5 Å square or a 6 Å diameter circle. If this proposed Ca^{2+} channel pore model has the correct dimensions, then its selectivity filter should accommodate TMA. The structure shown in Figure 6 forms a selectivity filter ∼5−6 Å in diameter, exactly the correct size to allow TMA to pass through. This is because the side chains of the Glu residues are flexible, and electrostatic repulsion keeps their side chain carboxylates as far apart as possible. When divalent ions are not present to offset the field, the Glu side chains are directed away from the pore and the selectivity filter is open to the passage of molecules smaller than 6 Å. In this sense, the pore of the Ca^{2+} channel inside the selectivity filter is normally open so that the channel in the absence of external Ca^{2+} is quite unselective (*49*).

In this construction, the outer vestibule of the Ca^{2+} channel pore is 18 Å deep, with a conical configuration that tapers from a top diameter of ∼20 Å to the narrow 6 Å selectivity filter at the bottom (Figures 5 and 6). All four P loops penetrate the membrane to the same depth. The selectivity filter is formed by the side chains of glutamic acids of the EEEE locus. The EEEE residues are arranged approximately on the same horizontal level relative to the axis of the pore. This model therefore produced a single binding site with optimal stereochemical conditions for the interaction of four Glu residues with the one Ca^{2+}.

Ca^{2+} Permeation. Permeation of cationic ions through the Ca^{2+} channel is very specific. The channel is highly permeable to Na^+ or Li^+ in the absence of divalent ions. Ca^{2+} blocks the monovalent currents with an affinity of ∼1 μM, and Ca^{2+} current itself develops in a saturable fashion only in the millimolar range (*3*). This has been explained as Ca^{2+} occupying a high-affinity site in the pore in the micromolar range, blocking the monovalent current. The bound Ca^{2+} does not permeate because of its high affinity. When the concentration of Ca^{2+} is increased to the millimolar range, it is proposed that a second Ca^{2+} binds to another high-affinity site in the pore, destabilizing the first one by electrostatic repulsion (*16*, *17*). This phenomenon has been studied intensively, and several points are clear. First of all, there is only a single high-affinity site comprised of the four glutamic acids in the selectivity ring, rather than two independent sites. Pairwise replacement of these four glutamate residues with alanine in all six possible combinations (E393A/E736A, E393A/E1145A, etc.) exhibited greatly reduced affinity (∼200−500-fold) for Ca^{2+} block of Li^+ current in each of the double mutants (*22*). If two independent high-affinity sites existed, then one or more of the double mutant channels should have shown high-affinity block of monovalent current without divalent current, but this was not observed. Consequently, all four glutamic acid residues must participate simultaneously in direct interactions in the single high-affinity site. Replacement of single glutamate residues with glutamine or alanine weakened the high-affinity Ca^{2+} interaction differently. In general, substitutions in domains II and III produced stronger effects than substitutions in domains I and IV, suggesting asymmetry of the P loops (*18*−*20*, *22*). However, for the same $Ca_v1.2$ channel, Parent and Gopalakrishnan (*23*) found that glutamates of domains III and IV are most crucial for Ca^{2+} binding, and that the glutamate of domain II is relatively neutral. In any case, the changes in energy predicted by these differences are relatively small. For example, substitutions of individual glutamates in all four domains with Gln reduced affinity by only 0.5−1.5 kcal/mol (*22*). Consequently, it is reasonable to consider the selectivity filter of Ca^{2+} channels as a quasi-symmetrical arrangement of the four glutamates. The selectivity filter also presents a single narrow aperture across the membrane, because Ca^{2+} shows block at the same field level, whether it arrives from the inside or the outside (*50*).

A pore with only one high-affinity site would not permit Ca^{2+} current (*51*); under such conditions, flux would be only about 50 s^{-1} (*51*, *52*). It is therefore necessary to include

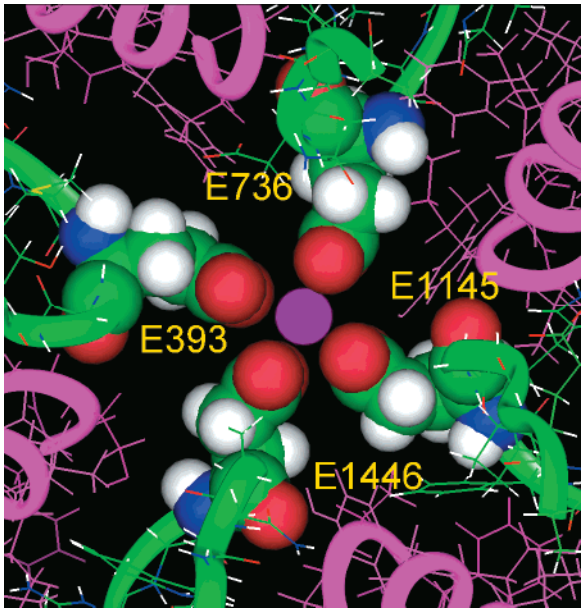

FIGURE 7: High-affinity binding site of Ca^{2+} inside the pore of the Ca^{2+} channel. In the presence of ~1 μM Ca^{2+}, all four glutamate side chains (shown by balls) of the selectivity filter move to the center of the pore and simultaneously interact in their extended conformations with a single Ca^{2+} ion (violet ball).

the presence of other low-affinity binding sites for Ca^{2+} inside the pore. Indeed, ion−ion interactions are present in the Ca^{2+} channel pore, because the direction of exit of the blocking Ca^{2+} is always with, not against, the Li^+ current (*53*). Experimental observations have shown that the pore can bind several, at least three, Ca^{2+} ions (*50*, *54*). Lower-affinity sites for monovalent or divalent binding can be identified on both sides of the high-affinity site when divalent concentrations are relatively low (*50*, *53*, *55*). Recognition of the presence of low-affinity sites led to the conclusion that permeation of Ca^{2+} through the pore is accompanied by stepwise changes in binding affinity (*52*).

How might the glutamates function in a quasi-symmetrical selectivity filter, as developed in the model? The model selectivity ring forms a wide open pore in the absence of divalent ions because of the electric field generated by these negatively charged residues, moving their side chains away from the pore center (Figures 5 and 6). In the presence of ~1 μM Ca^{2+}, the pore is occupied by a single Ca^{2+} ion (see refs *16* and *17*). We propose that all four glutamate side chains move to the center and simultaneously participate in similar direct interactions with the single dehydrated Ca^{2+} ion (Figure 7). The interactions are considered to be direct because substitution of any single glutamate with the shorter aspartate weakened the interactions with Ca^{2+}, as expected if there were direct ligand coordination rather than through-space electrostatic interaction (*22*). In this interaction, the carboxylate groups occupy vertical positions and both oxygens of each glutamate interact with Ca^{2+} employing the bidentate mode (*56*), so the high-affinity site contains eight oxygens that represent a possible Ca^{2+} ion coordination site. Separation of the P loops inside the outer vestibule (Figure 6) determines the distance between the carboxylate oxygens and Ca^{2+} of ~2.8−2.9 Å, within the limits of Ca−O distances found for bidentate binding in proteins (*57*). In this manner, the binding of Ca^{2+} ions creates a definite structure for the selectivity filter, which does not exist in its absence.

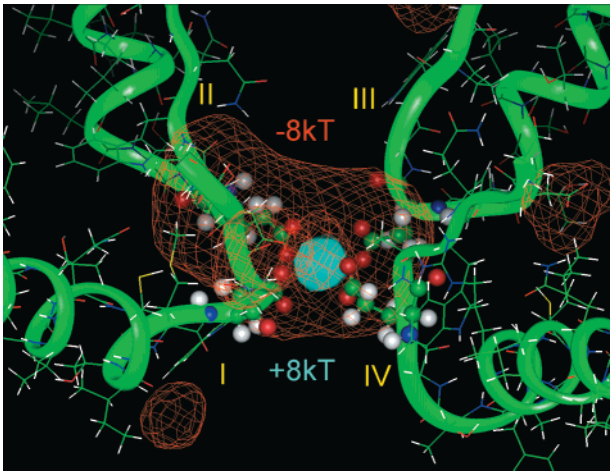

FIGURE 8: Electrostatic fields in the complex of the pore of the Ca^{2+} channel with one Ca^{2+} inside of the selectivity filter. Contours are shown at the 8 kT level with blue signifying positive and red signifying negative potentials; −8 kT corresponds to the deepest negative potential surrounding the positive potential produced by the single Ca^{2+} ion. Separated P loops are shown as green ribbons.

At the same time, this model presents a blocking state of the Ca^{2+} channel, inhibiting Ca^{2+} flux. Calculation of the electrostatic field for the complex of the pore containing one Ca^{2+} inside (Figure 8) shows the positive potential (blue contour) created by the Ca^{2+}, surrounded by the negative electrostatic field (red contour) created by the four carboxylate groups of the selectivity filter, placing Ca^{2+} in an electrostatic trap. In this calculation, each carboxylate was assumed to have one net negative charge.

The proposed binding of Ca^{2+} by radially symmetrical carboxylate groups from the four domains is different from Ca^{2+} binding in typical high-affinity sites (*56*, *57*). Typically, Ca^{2+} is bound in a seven-coordinate pentagonal bipyramidal geometry, where coordinating oxygens surround the ion in a spherical manner. However, there is precedent. In the bacteriophage ΦX174, Ca^{2+} is located at the center of a 5-fold symmetry axis and interacts with aspartate side chains from each of the five domains of the phage G protein (*58*). Furthermore, the symmetrical binding pattern offers the opportunity for displacement of the Ca^{2+} by external or internal ions.

The high-affinity site has been shown experimentally to be flanked by low-affinity sites in the permeation path, located internally (*50*) and externally (*55*). When the structural possibilities for formation of the low-affinity binding sites are considered, it is logical to expect that these low-affinity sites are also formed by the same four glutamates, since no alternative candidates are found in this region. $Ca_v1.2$ does contain an Asp at position 737, just above the selectivity filter Glu of domain II, where it might participate in the selectivity process. It and other carboxyls on the C-ends of P loops (Figure 1), which are also inside of the vestibule, were shown by mutation not to affect Ca^{2+} block of Li^+ currents (*19*, *23*). Previously, Armstrong and Neyton (*59*) also proposed that a high-affinity binding site containing one Ca^{2+} can interact weakly with a second incoming Ca^{2+}. To identify the origin of these lower-affinity sites, we need to consider the lone pair electrons of the two oxygen atoms of the carboxylate groups, where syn pairs are directed inside and anti pairs are directed outside (*56*). At low Ca^{2+}

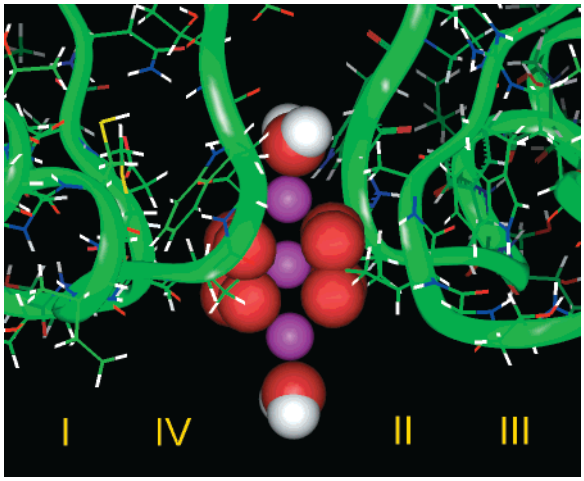

FIGURE 9: Binding of three Ca^{2+} ions (violet balls) inside the selectivity filter of the Ca^{2+} channel in the millimolar external Ca^{2+} concentration range. The central high-affinity site is flanked by two lower-affinity sites in the permeation path located externally and internally, and formed by the same four glutamate residues of the EEEE motif (their oxygens are shown as red balls). Ca^{2+} ions in the low-affinity sites are only partially dehydrated.

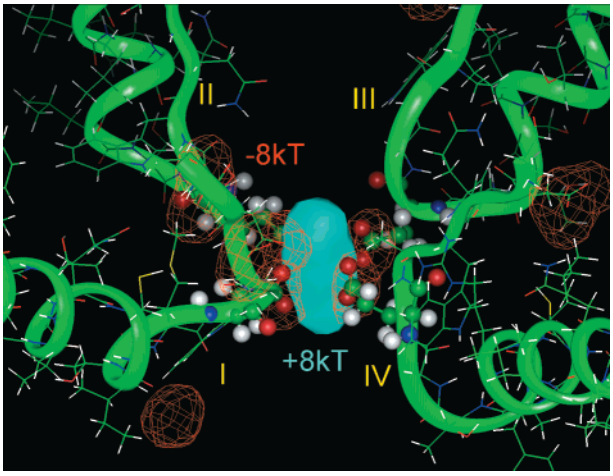

FIGURE 10: Electrostatic fields of the pore of the Ca^{2+} channel with occupation of the high-affinity and two low-affinity sites by three Ca^{2+} ions. In this situation, the four glutamate side chains cannot form an electrostatic trap, permitting Ca^{2+} flux through the pore (central positive electrostatic potential shown in blue).

concentrations, only the syn lone pair electrons of the eight oxygens interact with the Ca^{2+} in the central position, producing the high-affinity cage (Figure 7). An increase in the outside Ca^{2+} concentration into the millimolar range initiates interactions between the anti lone pairs of the upper four oxygens and the second Ca^{2+}, most likely in a partially dehydrated state. In the same fashion, there is a similar interaction with the lower four oxygens on the internal side of the pore, where partial rehydration of Ca^{2+} can occur on exit from the central position. Consequently, the proposed conformation of the selectivity filter containing the four glutamates could form three sites (Figure 9), a high-affinity site flanked by two lower-affinity sites. The calculated electrostatic interaction for the middle Ca^{2+} ion is 3 times stronger than corresponding energies for additional Ca^{2+} ions, as a consequence of the oxygen arrangement. An example where the carboxylate groups of two glutamic acids participate in bidentate binding with one Ca^{2+}, and simultaneously in unidentate binding with another Ca^{2+}, is found in the X-ray structure of thermolysin (*60*).

Occupancy of the first lower-affinity site can destabilize the adjacent high-affinity site. This newcomer Ca^{2+} can then function as an "enhancer" of displacement of the Ca^{2+} bound in the higher-affinity site, increasing its occupancy of the lower site formed by the lone anti pairs of electrons of the lower oxygens of the carboxylate groups. Alternatively, this anti interaction could provide a site for monovalent ions for "lock-in" or "enhancement" of flux (*53*). The movement of Ca^{2+} from the high-affinity site to the next internal site with intermediate affinity as the result of electrostatic repulsion eases exit of Ca^{2+} from the pore. Without these energetic stairsteps, the exit barrier from the high-affinity site would be very high, ~25 kcal/mol (*52*). The electrostatic field of the complex with three Ca^{2+} ions bound simultaneously in the three sites is shown in Figure 10. In the case of a single bound Ca^{2+}, the negative electrostatic potential of the pore holds Ca^{2+} inside (Figure 8); three Ca^{2+} ions are able to overcome electrostatic attraction of the four carboxylate groups, and one can leave the selectivity area. In this situation, the four glutamates cannot form an electrostatic trap, permitting Ca^{2+} flux. The occupancy of the pore by three Ca^{2+} ions when the concentration is in the millimolar range is in accordance with previous experiment (*50*, *54*).

One of the assumptions of this simplified model is that the P loops of both Na^+ and Ca^{2+} channels are arranged symmetrically to form planar selectivity regions. Considerable functional studies challenge this symmetry, and suggest that the P loops are at different depths in the pore or that each P loop has a different secondary structure (*61*, *62*). However, simultaneous participation of four carboxylate groups in Ca^{2+} binding tolerates a relative shift of 1−2 Å along the pore, corresponding to the change from bidentate to unidentate binding. Modest displacement of glutamates from the planar, symmetrical arrangement in this model would be sufficient to produce small differences in electrostatic interactions of each carboxylate with Ca^{2+} and to explain the nonuniform results of mutations (*19*, *22*, *23*). Alternatively, the asymmetrical behavior could result from the influence of residues adjacent to the glutamates, altering their reactivity or flexibility (*63*). The expected asymmetry of the pore residues is at this point beyond the limits of structural resolution; for example, the KcsA structure was determined with 3.2 Å resolution.

Nonner et al. (*64*) recently presented an ion exchange model of the Ca^{2+} channel selectivity process. Using a version of the Debye−Huckel equations incorporating ionic size, they demonstrated that eight oxygens, each with a negative half-charge, located in a restricted volume could discriminate between monovalent and divalent cations received from adjacent compartments with physiological salt solutions by opposing electrostatic attractive and van der Waals exclusion forces. They predicted binding ratios reproducing the biphasic pattern of ionic currents experimentally generated by addition of Ca^{2+} or Ba^{2+} to monovalent cation solutions. The model placed no constraint on the exact location of the oxygens, except that they remain in the assigned volume. The assumption of a continuous medium was confirmed by Monte Carlo simulations in a similar model of oxygens and ions in a restricted space (*65*).

The oxygens used in those simulations must be pairs derived from carboxylates, which have a relatively fixed geometry. The volume is determined by the flexibility of the tethered carboxylates and their proximity. Using coordinates and structural motifs derived from the KcsA crystal structure, analogy to the Na^+ channel vestibule, and limited mutational experiments, we have predicted an exact structure of the selectivity region of the Ca^{2+} channel that satisfies the geometrical requirements of the models of Nonner et al. (*64*) and Buda et al. (*65*). Carboxylates are tethered to a rigid backbone ring such that they may spontaneously coordinate with at least three cations of appropriate dimensions without creating a coordinate shell for Ca^{2+} such as is found in chelators. In the absence of divalent ions, the carboxylates can retract to provide a sieving pattern for large organic molecules. Our model offers a realistic geometry for the selectivity of the Ca^{2+} channel, and it may be useful in further exploration of the ion exchange model, including protons and water molecules.

Modeling Summary. We tested the idea that the P loop motif and the M1−M2 teepee motif and coordinates of the KcsA channel crystal structure could be applied to the Ca^{2+} channel pore, analogous to the Na^+ channel model we developed using similar logic. The channel P loops could be constructed with the α-helix−turn−β-strand motif that was successful for the Na^+ channel in preserving the characteristics of the multivalent guanidinium toxin binding sites. Phenylalkylamine interactions with the inner pore were used to align the S6 helical residues, and the S5 and S6 helices could then be assembled with the KcsA helical coordinates. The P loop structures could be docked into the teepees, locating the selectivity filter just outside the residues involved in the inner drug sites. In this model, the outer vestibule is formed by elements of the P loops and the S6 helices, with the S6 structures setting limits on the dimensions of the selectivity filter. Ca^{2+} channel selectivity occurs at a single site formed by the four glutamates of the EEEE motif. It can bind one Ca^{2+} with high affinity, but it also provides for two adjacent lower-affinity cation sites. In the millimolar external Ca^{2+} concentration range, binding of three Ca^{2+} ions simultaneously to the high-affinity site and the two low-affinity ones is necessary to overcome the electrostatic trap and permit flux through the pore of the Ca^{2+} channel.

REFERENCES

1. Doyle, D. A., Cabral, J. M., Pfuetzner, R. A., Kuo, A., Gulbis, J. M., Cohen, S. L., Chait, B. T., and MacKinnon, R. (1998) *Science 280*, 69−74.
2. Lipkind, G. M., and Fozzard, H. A. (2000) *Biochemistry 39*, 8161−8170.
3. Hille, B. (1992) *Ionic Channels of Excitable Membranes*, 2nd ed., Sinauer, Sunderland, MA.
4. Goldin, A. L. (1994) in *Handbook of Receptors and Channels* (North, R. A., Ed.) Vol. II, pp 73−112, CRC Press, Boca Raton, FL.
5. Catterall, W. A. (1995) *Annu. Rev. Biochem. 64*, 493−531.
6. Fozzard, H. A., and Hanck, D. A. (1996) *Physiol. Rev. 76*, 887−926.
7. Guy, H. R., and Conti, F. (1990) *Trends Neurosci. 13*, 201−206.
8. Hockerman, G. H., Peterson, B. Z., Johnson, B. D., and Catterall, W. A. (1997) *Annu. Rev. Pharmacol. Toxicol. 37*, 361−396.
9. Terlau, H., Heinemann, S. M., Stühmer, W., Pusch, M., Conti, F., Imoto, K., and Numa, S. (1991) *FEBS Lett. 293*, 93−96.
10. Favre, I., Moczydlowski, E., and Schild, L. (1996) *Biophys. J. 71*, 3110−3132.
11. Schlief, T., Schonherr, R., Imoto, K., and Heinemann, S. H. (1996) *Eur. Biophys. J. 25*, 75−91.
12. Penzotti, J. L., Lipkind, G. M., Fozzard, H. A., and Dudley, S. C. (1998) *Biophys. J. 75*, 2647−2657.
13. Armstrong, C., and Hille, B. (1998) *Neuron 20*, 371−380.
14. Heinemann, S. M., Terlau, H., Stühmer, W., Imoto, W., and Numa, S. (1992) *Nature 356*, 441−443.
15. Stea, A., Soong, T. W., and Snutch, T. P. (1994) in *Handbook of Receptors and Channels* (North, R. A., Ed.) Vol. II, pp 113−152, CRC Press, Boca Raton, FL.
16. Hess, P., and Tsien, R. W. (1984) *Nature 309*, 453−456.
17. Almers, W., and McCleskey, E. W. (1984) *J. Physiol. 353*, 585−608.
18. Tang, S., Mikala, G., Bahinski, A., Yatani, A., Varadi, G., and Schwartz, A. (1993) *J. Biol. Chem. 268*, 13026−13029.
19. Yang, J., Ellinor, P. T., Sather, W. A., Zhang, J.-F., and Tsien, R. W. (1993) *Nature 366*, 158−161.
20. Kim, M. S., Morii, T., Sun, L. X., Imoto, K., and Mori, Y. (1993) *FEBS Lett. 318*, 145−148.
21. Mikala, G., Bahinski, A., Yatani, A., Tang, S., and Schwartz, A. (1993) *FEBS Lett. 335*, 265−269.
22. Ellinor, P. T., Yang, J., Sather, W. A., Zhang, J.-F., and Tsien, R. W. (1995) *Neuron 15*, 1121−1132.
23. Parent, L., and Gopalakrishnan, M. (1995) *Biophys. J. 69*, 1801−1813.
24. Wu, X., Edwards, H. D., and Sather, W. A. (2000) *Biophys. J. 78*, 456A.
25. Catterall, W. A. (1992) *Physiol. Rev. 72* (Suppl.), S15−S48.
26. Lipkind, G. M., and Fozzard, H. A. (1994) *Biophys. J. 66*, 1−13.
27. Satin, J., Kyle, J. W., Chen, M., Bell, P., Cribbs, L. L., Fozzard, H. A., and Rogart, R. B. (1992) *Science 256*, 1202−1205.
28. Kao, C. Y. (1986) *Ann. N.Y. Acad. Sci. 479*, 52−67.
29. MacKinnon, R., Cohen, S. C., Kuo, A., Lee, A., and Chait, B. T. (1998) *Science 280*, 106−109.
30. Gilson, M. K., and Honig, B. H. (1987) *Nature 330*, 84−86.
31. Dudley, S. C., Chang, N., Hall, J., Lipkind, G. M., Fozzard, H. A., and French, R. J. (2000) *J. Gen. Physiol. 116*, 679−689.
32. Creighton, T. E. (1993) *Proteins: Structures and Molecular Properties*, 2nd ed., W. H. Freeman and Co., New York.
33. Varadi, G., Mori, Y., Mikala, G., and Schwartz, A. (1995) *Trends Pharmacol. Sci. 16*, 43−49.
34. Hsu, K., Amzel, M., Tomaselli, G., and Marban, E. (1999) *Biophys. J. 76*, A82.
35. Rice, P. A., Goldman, A., and Steitz, T. A. (1990) *Proteins 8*, 334−343.
36. Efimov, A. V. (1993) *Prog. Mol. Biol. 60*, 201−239.
37. Chou, P. V., and Fasman, G. D. (1978) *Annu. Rev. Biochem. 47*, 251−276.
38. Banner, D. W., Bloomer, A. C., Petsco, G. A., Phillips, D. C., Pogson, C. L., and Wilson, I. A. (1975) *Nature 255*, 609−612.
39. Hockerman, G. H., Johnson, B. D., Scheuer, T., and Catterall, W. A. (1995) *J. Biol. Chem. 270*, 22119−22122.
40. Hockerman, G. H., Johnson, B. D., Abbott, M. R., Scheuer, T., and Catterall, W. A. (1997) *J. Biol. Chem. 272*, 18759−18765.
41. Dudley, S. C., Jr., Todt, H., Lipkind, G., and Fozzard, H. A. (1995) *Biophys. J. 69*, 1657−1665.
42. Chang, N. S., French, R. J., Lipkind, G. M., Fozzard, H. A., and Dudley, S. C., Jr. (1998) *Biochemistry 37*, 4407−4419.
43. Ragsdale, D. S., McPhee, J. C., Scheuer, T., and Catterall, W. A. (1994) *Science 265*, 1724−1728.
44. Peterson, B. Z., Johnson, B. D., Hockerman, G. H., Acheson, M., Scheuer, T., and Catterall, W. A. (1997) *J. Biol. Chem. 272*, 18752−18758.

45. Peterson, B. Z., and Catterall, W. A. (1995) *J. Biol. Chem. 270*, 18201−18204.
46. Mitterdorfer, J., Sinnegger, M. J., Grabner, M., Striessnig, J., and Glossmann, H. (1995) *Biochemistry 34*, 9350−9355.
47. McCleskey, E. W., and Almers, W. (1985) *Proc. Natl. Acad. Sci. U.S.A. 82*, 4328−4331.
48. Coronado, R., and Smith, J. S. (1987) *Biophys. J. 51*, 497−502.
49. Yellen, G. (1993) *Nature 366*, 109−110.
50. Kuo, C.-C., and Hess, P. (1993) *J. Physiol. 466*, 629−655.
51. McCleskey, E. W. (1999) *J. Gen. Physiol. 113*, 765−772.
52. Dang, T. X., and McCleskey, E. W. (1998) *J. Gen. Physiol. 111*, 185−193.
53. Kuo, C.-C., and Hess, P. (1993) *J. Physiol. 466*, 657−682.
54. Yue, D. T., and Marban, E. (1990) *J. Gen. Physiol. 95*, 911−939.
55. Polo-Parada, L., and Korn, S. (1997) *J. Gen. Physiol. 109*, 693−702.
56. Glusker, J. P. (1991) *Adv. Protein Chem. 42*, 1−76.
57. Falke, J. J., Drake, S. K., Hazard, A. L., and Peerson, O. B. (1994) *Q. Rev. Biophys. 27*, 219−290.
58. McKenna, R., Xia, D., Willingmann, P., Ilag, L. L., Krishnaswamy, S., Rossman, M. G., Olson, N. H., Baker, T. S., and Incardona, N. L. (1992) *Nature 335*, 137−143.
59. Armstrong, C. M., and Neyton, J. (1992) *Ann. N.Y. Acad. Sci. 635*, 18−25.
60. Matthews, B. W., Weaver, L. H., and Kester, W. R. (1974) *J. Biol. Chem. 249*, 8030−8044.
61. Perez-Garcia, M. T., Chiamvimonvat, N., Marban, E., and Tomaselli, G. F. (1996) *Proc. Natl. Acad. Sci. U.S.A. 93*, 300−304.
62. Benitah, J.-P., Ranjan, R., Yamagishi, T., Janecki, M., Tomaselli, G. F., and Marban, E. (1997) *Biophys. J. 73*, 603−618.
63. Williamson, A. V., and Sather, W. A. (1999) *Biophys. J. 77*, 2575−2589.
64. Nonner, W., Catacuzzeno, L., and Eisenberg, R. S. (2000) *Biophys. J. 79*, 1976−1992.
65. Boda, D., Busath, D. D., Henderson, D., and Sokolowski, S. (2000) *J. Phys. Chem. B 104*, 8903−8910.

BI010269A